Available online at www.sciencedirect.com
ScienceDirect
International Journal of Heat and Mass Transfer 50 (2007) 1916–1926
International Journal of HEAT and MASS TRANSFER
www.elsevier.com/locate/ijhmt

Forced convective heat transfer with impinging rectangular jets

D.W. Zhou [a,b,*], Sang-Joon Lee [a]

[a] Department of Mechanical Engineering, Pohang University of Science and Technology, Pohang 790-784, Republic of Korea
[b] Department of Mechanical and Aerospace Engineering, Arizona State University, Tempe, AZ 85287-6106, United States

Received 3 February 2006; received in revised form 30 September 2006
Available online 27 November 2006

Abstract

The fluid flow and heat transfer characteristics of a rectangular air jet impinging on a heated flat plate have been investigated experimentally. The effects of jet Reynolds number and nozzle-to-plate spacing on local and average Nusselt number were studied. Results show that both have a significant influence on heat transfer behaviors of impinging jets. Local and average heat transfer data along the axial and lateral directions were correlated and compared with the previous data. The local *Nu* number and the free-stream turbulence intensity of impinging jets exhibit a relationship:

$$Nu/Re^{1/2} = 0.014 Tu Re^{1/2} + 0.517.$$

The corresponding average *Nu* number and turbulence intensity have a relationship:

$$\overline{Nu}/Re^{1/2} = 0.014 \overline{Tu} Re^{1/2} + 0.472.$$

Heat transfer mechanics was analyzed in terms of the turbulence intensity.

Keywords: Rectangular jet impingement; Heat transfer; Turbulence intensity; Convection

1. Introduction

Impinging jets are encountered in a wide range of industrial processes as an efficient means to enhance and control localized heat and mass transfer. Applications of impinging jets include drying of textiles, film, and paper; cooling of gas turbine components and the outer wall of combustors; freezing of tissue in cryosurgery; and cooling of electronic equipment. Significant attention has been paid to impinging jets and the high heat and mass transfer rates associated with impinging gaseous jets have been well recognized and documented [1,2]. The majority of these studies have been related to single circular jets or rows of single jets.

Circular jets and slot jets are two basic jet configurations employed in the existing study. However, they have distinctly different fluid flow and heat transfer mechanics. From the survey of existing literature, a single circular jet concentrates cooling only in the small impingement zone of the heated surface [3,4]. Compared to circular jets, slot jets obviously offer some beneficial features, such as higher heat and mass transfer rate, greater uniformity and more controllability [5]. Clearly, these factors are believed to challenge a continuously increasing heat flux and decreasing dimensions in compact electronics packages.

The heat transfer rate on the impingement surface has a close relationship with flow structure at the nozzle exit. Very little work reported the fluid flow and heat transfer rate of impinging slot jets. Schwarz and Cosart [6] presented measurements and an analysis on the fluid flow characteristics of impinging slot jet, but only for the turbulent wall jet zone. Gardon and Akfirat [7] investigated the

* Corresponding author. Present address: Department of Mechanical and Aerospace Engineering, Arizona State University, Tempe, AZ 85287-6106, United States. Tel.: +1 480 965 8482; fax: +1 480 965 1384.
E-mail address: drdwzhou@hotmail.com (D.W. Zhou).

0017-9310/$ - see front matter © 2006 Elsevier Ltd. All rights reserved.
doi:10.1016/j.ijheatmasstransfer.2006.09.022

Nomenclature

A	area of gold-coated film (heating area)	Re	jet Reynolds number, uB/v
B	slot width	T_j	jet exit temperature
C_0	velocity gradient, Eq. (3)	T_w	local wall temperature
C_1, C_2	coefficient, Eqs. (9) and (12)	Tu	local RMS velocity fluctuation, $\frac{\sqrt{\overline{u'^2}}}{U_e}$
f	non-uniformity factor of gold-coated film	U	local mean radial velocity
h	local heat transfer coefficient, Eq. (6)	U_c	local mean streamwise velocity on the jet centerline
I	electric current across the gold-coated film	U_e	jet exit velocity
k	thermal conductivity of air	u_δ	local free stream value of u, Eq. (3)
m_1, m_2	exponent, Eqs. (9) and (12)	V	voltage across the gold-coated film
n_1, n_2	exponent, Eqs. (9) and (12)	x	lateral distance from the stagnation line
Nu	local Nusselt number, Eq. (6)	X/B	dimensionless lateral distance
Nu_0	stagnation Nusselt number	z	distance between the nozzle exit and the impingement plate
$\overline{Nu}$	average Nusselt number	Z/B	dimensionless nozzle-to-plate spacing
q_c	conduction heat flux		
q_v	convection heat flux, Eq. (7)		

variation in local heat transfer rate produced by impinging slot jets with changes in the free stream turbulence at the nozzle exit. They concluded that some seemingly anomalous heat transfer phenomena could be explained in light of the turbulence intensity inherent in jets, and that slot jet with larger nozzle width produced higher heat transfer rate. Subsequently, they studied local and average heat transfer rate between an isothermal flat plate and impinging slot jets for both single jets and arrays jets [8]. In the range of $Re = 2000$–$50{,}000$ and $Z/B = 14$–60, stagnation heat transfer data are correlated within $\pm 5\%$ by

$$Nu_0 = 1.2Re^{0.58}(Z/B)^{-0.62}. \tag{1}$$

McMurray et al. [9] performed heat transfer measurements for both laminar and turbulent boundary layer and their correlation for laminar boundary layer is of the form

$$Nu_0 = 0.73Re^{1/2}Pr^{1/3}. \tag{2}$$

Using the naphthalene sublimation technique, Sparrow and Wong [10] studied the local mass transfer rate of a laminar slot jet impinging on a plane surface. Lin et al. [5] studied, experimentally and numerically, the fluid flow and heat transfer behaviors of a confined impinging slot jet for $1 < Z/B < 8$. For a semi-confined impinging slot jet, Ashforth-Frost et al. [11] obtained streamwise velocity and turbulence characteristics for $Z/B = 4$ and 9.2 at $Re = 20{,}000$. Their results showed that the velocity and turbulence data of impinging jet were directly related to the heat transfer.

Falkner and Skan's [12] analyses have shown that the parameter $C_0 = \mathrm{d}u_\delta/\mathrm{d}x$ controls stagnation heat transfer when the thermophysical properties are constant. Euler's equation for an impinging, finite width, slot jet with a uniform free stream velocity was evaluated to determine C_0

$$C_0 = \frac{\mathrm{d}u_\delta}{\mathrm{d}x} = \frac{\pi}{4}\frac{V_j}{w_j}, \tag{3}$$

where v_j and w_j are velocity and width of the impinging jet, respectively. An expression for the stagnation Nusselt number was derived by Vader et al. [13] and given below

$$Nu_0 = 0.505Re^{1/2}Pr^{0.376}. \tag{4}$$

For a laminar flow, Kendoush [14] studied theoretically the heat and mass transfer mechanics of an impinging slot jet by means of the boundary layer theory. The results were restricted just to the stagnation zone. The recommended correlation for the stagnation heat transfer rate is given below

$$Nu_0 = 0.75[RePr(1.02 - 0.024(Z/B))]^{1/2}. \tag{5}$$

Park et al. [15] numerically studied the fluid flow and heat transfer characteristics of confined impinging slot jets. The solutions for laminar and turbulent flow were available only for a limited range of jet Reynolds number.

Rectangular jet is a typical slot jet with smaller aspect ratio. Due to three-dimensional flow structure and complicated heat transfer distribution, there are very limited previous studies on impinging rectangular jet heat transfer. Using three different aspect ratios of 10, 20 and 30, Sfeir [16] measured the mean velocity and temperature profiles of rectangular jets. The flow-field, for both velocity and temperature, is found to be divided in three distinct regions: the potential core, the two-dimensional region and the axisymmetric region. These regions are not the same for the velocity and temperature distributions. The extent of each of these regions is a function of the nozzle aspect ratio. The flow in the two-dimensional region as well as the transition to axisymmetry is strong function of the nozzle geometry. At large distances from the nozzle exit, both the velocity and temperature fields are found to behave in the same way as that of the flow out of the circular nozzle of the same area. Quinn [17] studied the influence of aspect ratio on turbulent free jet flows issuing from sharp-edged rectangular jets. Four slot aspect ratios

(2, 5, 10 and 20) were used. The results indicate that, as the aspect ratio increases, the speed of mixing in the very near flow field increases while the potential core length decreases. The rectangular jet is now being used for thrust vectoring and enhanced mixing in the aerospace industry.

The objective of this study is to measure the flow structure and local heat transfer rate of an impinging rectangular jet. The experimental parameters include jet Reynolds number ($Re = 2715$–$25{,}005$) and nozzle-to-plate spacing ($Z/B = 1$–30). The mean velocity and turbulence intensity profiles of impinging free jets are measured using a hot-wire anemometry to understand the near-field flow structure. The present data are helpful for researcher and engineer to evaluate the flow structure and heat transfer characteristics of impinging rectangular jet and hence its optimum design.

2. Experimental apparatus and method

2.1. Jet flow system

A schematic diagram of the experimental apparatus is shown in Fig. 1. Compressed air passes through a heat exchanger, an orifice flowmeter, a flexible tube, a honeycomb and a long straight PVC pipe before entering a sharp-edged rectangular nozzle. A heat exchanger was installed to adjust the air temperature so that the jet exit temperature was maintained within ±0.1 °C of the ambient room temperature. The flow rate was measured with an ASME standard orifice flowmeter with ±1% reading accuracy. A circular straight PVC pipe with internal diameter of 52.3 mm and a length of 2.5 m was used. The pipe was rigidly mounted on a traversing fixture by which the nozzle-to-plate spacing could be adjusted with a resolution of 0.01 mm.

A sharp-edged rectangular nozzle was horizontally attached at the downstream end of the long pipe as shown in Fig. 2. The nozzle has a cross-section area of 44.2 mm × 11.08 mm with an aspect ratio of 4 and a thickness of 2 mm, respectively. This kind of sharp-edged nozzle has virtually zero momentum thickness at the nozzle exit. One thermocouple was installed using a feed-through hole at 20 mm upstream from the nozzle exit to measure the jet temperature. Another thermocouple was placed near the impingement region to monitor the ambient air temperature.

The heated impingement plate was composed of a Plexiglas flat plate, a gold-coated film, thirty-three T-type thermocouples and two copper electrodes. The Plexiglas plate of 303 × 303 mm^2 was 12.7 mm thick and had a low thermal conductivity. The transparent vacuum-deposited gold-coated film, 120 mm long by 40 mm wide, had a thickness of 127 μm and was glued to the Plexiglas plate. Two copper-foil strip electrodes with a thickness of 100 μm were attached to the film. Then, silver paint was applied to establish a good electrical contact between the electrode and the upper surface of the film. The electrodes were connected to a DC power supply (HP6555A) in series with a shunt, rated 50 mV and 5 A, allowing adjustable DC voltage to the electrodes. With DC electric current applied the film, a nearly uniform wall heat flux boundary condition was established. A HP3852A data acquisition system was used to measure the electric voltage drop across the film, current input to the shunt register and

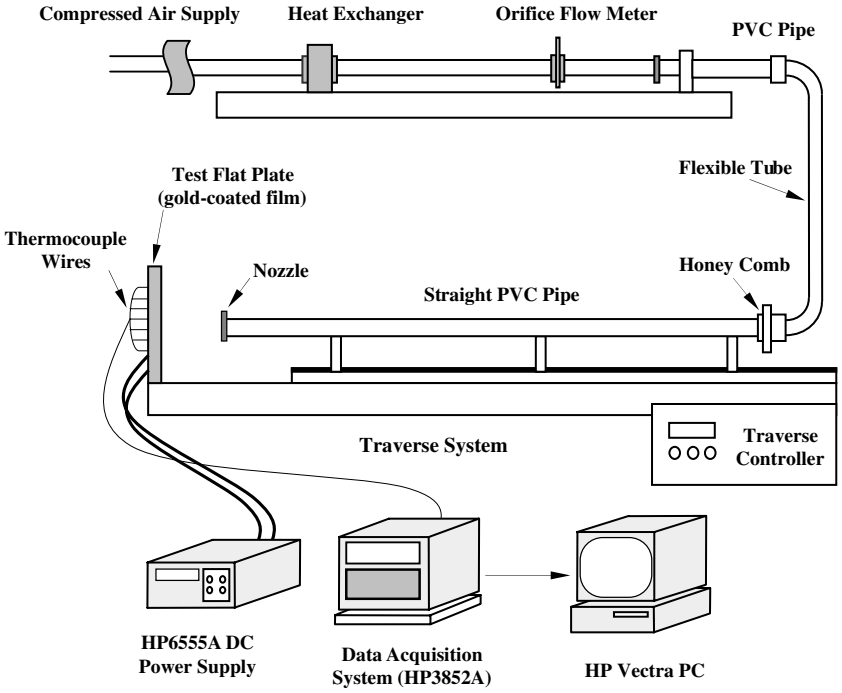

Fig. 1. Schematic diagram of experimental set-up.

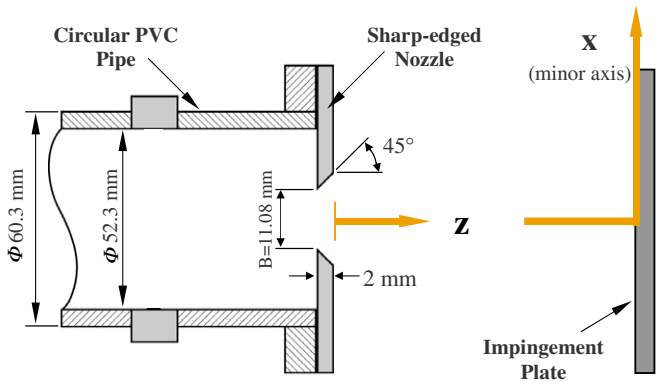

Fig. 2. Nozzle exit configuration and coordinate system.

the temperatures of all the thermocouples. Further details about the experimental apparatus and procedure can be found in Ref. [3].

2.2. Data reduction and uncertainty analysis

The local convective heat transfer rate and corresponding Nusselt number at a particular position were calculated using the following equations:

$$h = \frac{q_v}{(T_w - T_j)}, \quad Nu = \frac{hB}{k}, \tag{6}$$

where q_v is the convective heat flux, and k and T_j are the thermal conductivity of air and the jet exit temperature, respectively. Typical values for the temperature difference $(T_w - T_j)$ are in the range of 4–18 K for a uniform heat flux of 900 W/m^2 on the impingement plate. Each temperature was obtained by averaging 60 readings. All thermophysical properties in the non-dimensional parameters were all evaluated at the jet exit temperature. The convective heat flux q_v was obtained by subtracting the energy losses (q_c) from the total heat flux imposed on the gold-coated film and given by

$$q_v = \frac{fIV}{A} - q_c. \tag{7}$$

The lateral heat conduction was calculated by solving one-dimensional energy equation along the lateral direction of the plate, while the axial heat conduction was nearly negligible due to styrofoam insulation on the back side of the impingement plate and low thermal conductivity of the polyester substrate. The maximum conduction heat flux was estimated as about 2.8% of the total imposed heat flux. The radiation heat flux was calculated from Stefan-Boltzmann equation and found to be less than 0.5% of total imposed heat flux. In Eq. (7), f accounts for non-uniformity factor of the gold-coated film and $f \approx 1$ is usually adopted for small slender shape of the film. However, it contributes largely to the uncertainty in total Nusselt number evaluation. The average Nusselt number is defined as (Table 1)

$$\overline{Nu} = \frac{q_v B}{k(\overline{T_w - T_j})} = \left[\frac{2}{x^2}\int_0^x \frac{x\,dx}{Nu(x)}\right]^{-1}. \tag{8}$$

Table 1
Uncertainty analysis of the total Nusselt number

Individual measured value		$\left\lvert\frac{\delta x_i}{Nu}\frac{\partial Nu}{\partial x_i}\right\rvert \times 100\%$
x_i	Unit	
f	–	2.10–2.64
T_w	°C	1.57–2.25
V	V	0.65–1.17
I	A	0.42–1.29
q_c	W/m^2	0.18–2.11
T_a	°C	0.01–0.14
T_j	°C	0.01–0.11
B	m	0.11
A	m^2	0.08
k	W/m K	0.06

Total uncertainty : $\frac{\delta Nu}{Nu} = 2.92$–$3.87\%$

The integral equation was calculated using the Newton-Cotes formula with three-point correlation based on the measured Nu values.

The uncertainties were estimated using the method suggested by Kline and McClintock [18] with a 95% confidence level. The total uncertainties estimated for the local Nusselt number and the jet Reynolds number were in the range of 2.92–3.87% and 2.78%, respectively. The primary contributor comes from the non-uniformity factor f of the gold-coated film and its uncertainty ranges from 2.10% to 2.64%. The wall temperature T_w has uncertainty in the range of 1.57–2.25%. The measurement uncertainties estimated for the mean velocity and the turbulence intensity were less than 1.4% and 3.5%, respectively.

3. Results and discussion

3.1. Flow structure

To understand the flow structure of the impinging jet, the streamwise mean velocity and the turbulence intensity of the streamwise velocity component of the free jet (i.e., the component along the Z-axis) were measured. It should be noted here that both the fluid flow and heat transfer measurements have been carried out along the minor axis (X-axis in Fig. 2) of the jet. Since the impingement plate was removed for the hot-wire measurements, the nozzle-to-plate spacing indicates the distance between the nozzle exit and the tip of hot-wire probe.

The mean velocity and the turbulence intensity distributions at four downstream locations for $Re = 6500$ and 12,500 are compared in Fig. 3(a) and (b), respectively. As can be seen in Fig. 3, the general shape of the mean velocity and the turbulence intensity distributions for two jet Reynolds numbers is quite similar. Furthermore, a higher jet Reynolds number produces a larger mean velocity and turbulence intensity. Fig. 3(a) showed the normalized mean velocity distributions. At the downstream location of $Z/B = 1.0$ and a fixed jet Reynolds number, the mean velocity is approximately constant in the central region of the jet. The mean velocity decreases rapidly at

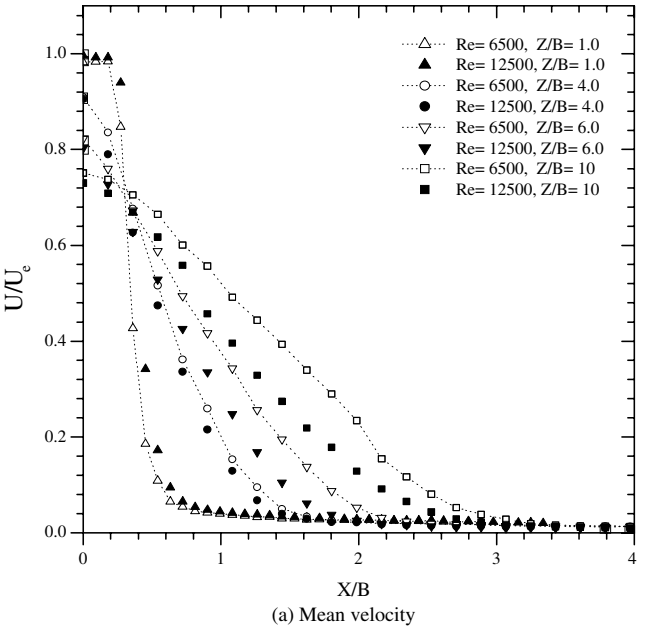

(a) Mean velocity

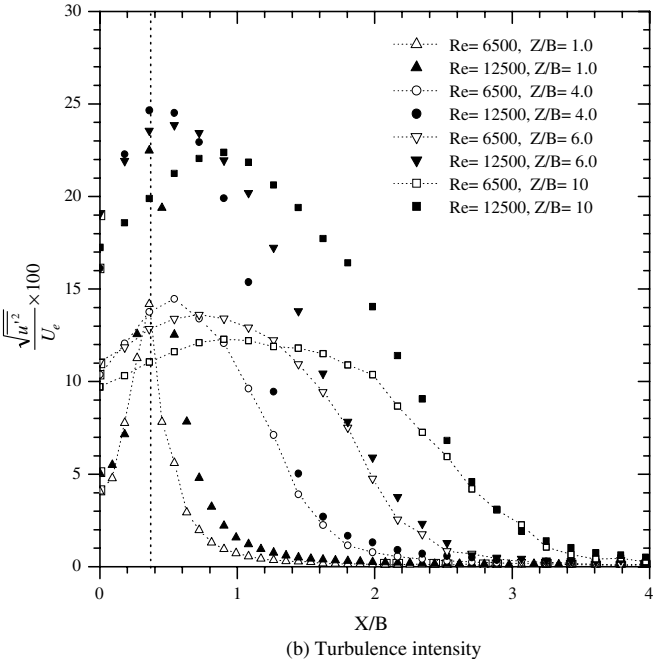

(b) Turbulence intensity

Fig. 3. (a, b) Variations of the mean velocity and turbulence intensity profiles with respect to the nozzle-to-plate spacing: (a) mean velocity (b) turbulence intensity.

$X/B = 0.4$-0.6, resulting from the vena contracta that commonly encountered in orifice jets. On moving downstream, however, the central region of the constant mean velocity is reduced and disappears at $Z/B = 4$. Thereafter, the mean velocity has a bell-shaped distribution. With going downstream, the maximum velocity at the jet center decreases and the jet flow stretches along the lateral direction. The effect of increasing jet Reynolds number manifests as an increase in the shear layer velocity gradient. As the flow goes downstream, the difference in axial mean velocity is increased. With the plate held at the $Z/B \leqslant 3$, the mean velocity for $Re = 12{,}500$ has a relative higher value. An opposite trend is seen for further downstream locations.

The lateral profile of the axial turbulence intensity corresponding to the mean velocity profiles of Fig. 3(a) is depicted in Fig. 3(b). At $Z/B = 1.0$, the turbulence intensity has a sharp peak at approximately $X/B = 0.36$ for two jet Reynolds numbers. It is always accompanied with a high velocity gradient in the shear layer shown in Fig. 3(a), resulting from a strong mixing between the potential core and the stagnant ambient fluid. The turbulence intensity decreases as the lateral distance varies. However, the center region of the jet remains high turbulence intensity. As the jet proceeds downstream, the turbulence intensity increases in the impingement region. This increase in turbulence intensity continues up to the downstream location of $Z/B = 6.0$, indicating that the jet flow has been, somewhat, fully developed. On going further downstream, the turbulence intensity decreases gradually. The turbulence intensity has its maximum value at the location of $Z/B = 2$ and $X/B = 0.36$. The lateral location of the maximum turbulence intensity shifts outward the centerline with going downstream. At further downstream, the sharp peak in the turbulence intensity distribution becomes blunt due to active mixing and turbulent diffusion. A higher turbulence intensity at $Z/B = 4.0$ and 6.0 indicates the jet has more vigorous velocity fluctuations there. Independent of the axial location, the turbulence intensity approaches at certain lateral location for two jet Reynolds number.

The mean velocity and the turbulence intensity profiles measured along the jet centerline for two jet Reynolds number are shown in Fig. 4(a) and (b). In this figure, all the data were non-dimensioned by the jet exit velocity U_e and the potential core length is 4 slot widths for two jet Reynolds numbers. The normalized velocity decreases gradually with an increasing nozzle-to-plate spacing, as shown in Fig. 4(a), independent of the jet Reynolds number. The jet for $Re = 12{,}500$ has a higher normalized velocity with comparison to the case of $Re = 6500$ as the nozzle-to-plate spacing is less than 4. The opposite trend occurs at the further downstream, indicating a strong mixing with the surrounding air there.

The variation in turbulence intensity along the jet centerline is shown in Fig. 4(b). For comparison, the results of Gardon and Akfirat [7] for $B = 6.35$ mm and $Re = 5500$ are included in the figure. The turbulence intensities increases rapidly with Z/B till up to $Z/B = 6$, where they have maximum values, and then decrease monotonically on going further downstream. The present results show a similar trend to those of Gardon and Akfirat [7], although the magnitudes and peak locations are different. These discrepancies may be primary attributed to differences in nozzle width and nozzle configuration. Their results show a peak value at $Z/B = 7.4$ for contoured nozzle and the peak location shift to upstream location with increasing slot width. In the present study with a sharp-edged rectangular nozzle, however, the peak occurs at the same location of $Z/B = 6$ for two jet Reynolds numbers.

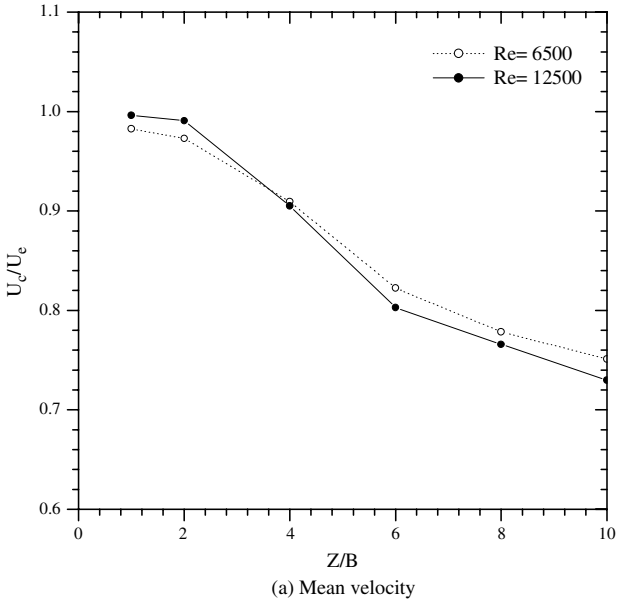

(a) Mean velocity

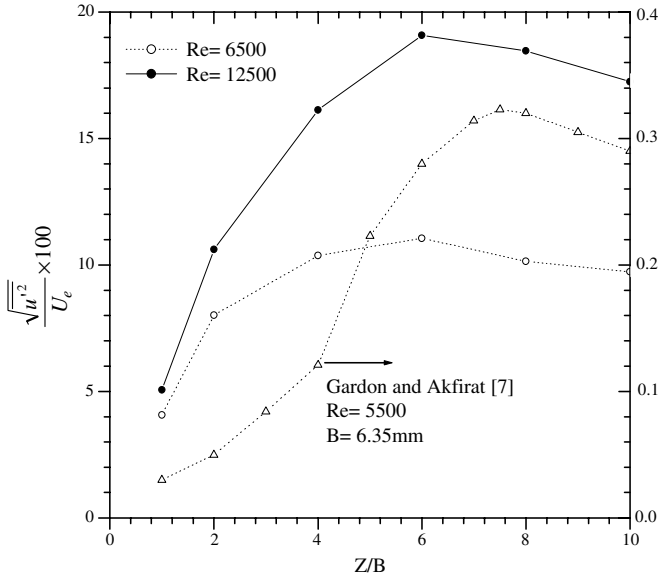

(b) Turbulence intensity

Fig. 4. (a, b) Mean velocity and turbulence intensity distributions along the jet centerline for different jet Reynolds numbers: (a) mean velocity (b) turbulence intensity.

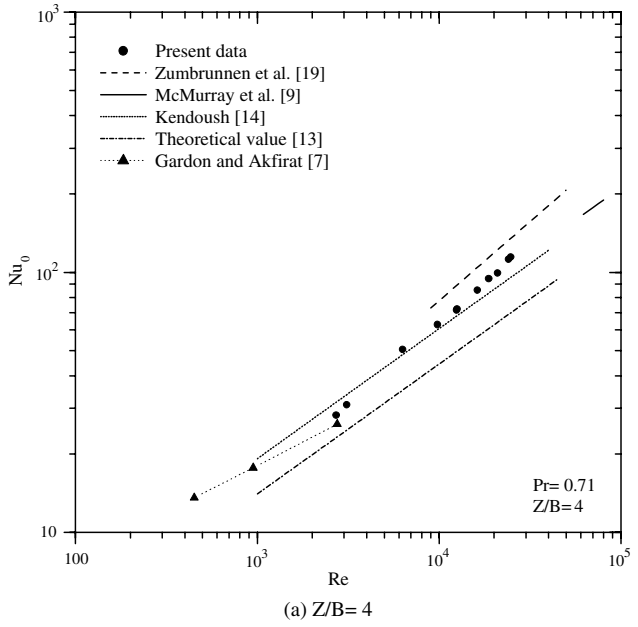

(a) Z/B= 4

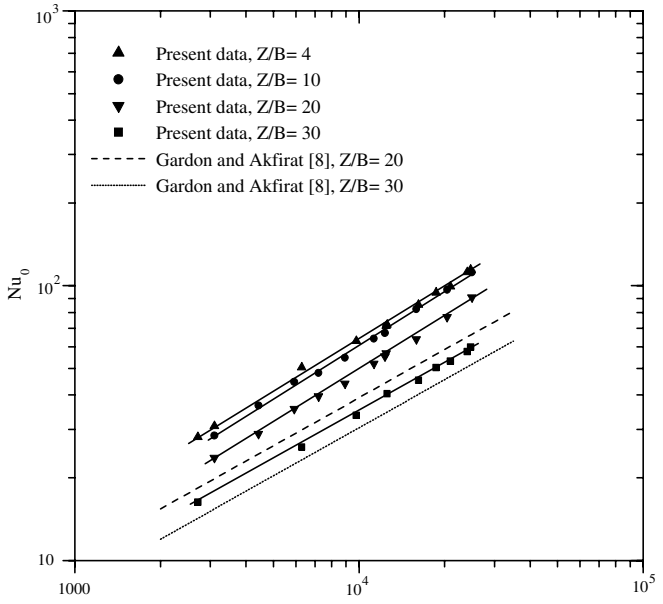

(b) Z/B= 4, 10, 20 and 30

Fig. 5. (a, b) Correlation and comparison of the stagnation Nusselt number: (a) $Z/B = 4$ (b) $Z/B = 4$, 10, 20 and 30.

With the increase of the jet Reynolds number, the turbulence intensity increases significantly.

3.2. Heat transfer characteristics

For jet Reynolds number in the range $2715 \leqslant Re \leqslant 25{,}005$, the stagnation Nusselt number were examined at four fixed nozzle-to-plate spacing of 4, 10, 20 and 30 and compared with the previous experimental and theoretical results as a validation process. The results are shown in Fig. 5(a) and (b). Fig. 5(a) exhibits the variation of the stagnation Nusselt number obtained at $Z/B = 4$ with jet Reynolds number, in which comparison of several empirical correlations of stagnation heat transfer from the work of Gardon and Akfirat [7], McMurray et al. [9], Zumbrunnen et al. [19], Vader et al. [13] and Kendoush [14] are also plotted. In this figure, the calculation was carried out at $Z/B = 4$ and the Prandtl number of air ($Pr = 0.71$) was adopted for all the correlations. Good agreements between the present data and the previous experimental and theoretical results were observed. The present value is 18–20% lower than that of Zumbrunnen et al. [19] for $B =$ 10.2 mm. This is believed to be mainly attributed to the different turbulence level of the jet flow. The turbulence intensity in the free jet changes with jet Reynolds number,

fluid Prandtl number, nozzle configuration [3] and slot width [7]. The present data is 17–35% greater than the analytical results of Eq. (3) [13] for a laminar, impinging jet, and slightly greater than the result reported by Gardon and Akfirat [7] with $B = 6.35$ mm.

Fig. 5(b) illustrates the variation of the stagnation Nusselt number with respect to jet Reynolds number for four nozzle-to-plate spacing of $Z/B = 4$, 10, 20 and 30. As shown in the figure, there is a distinct nozzle-to-plate spacing dependence in the functional relationship of stagnation Nusselt number with jet Reynolds number. Higher stagnation heat transfer rates were observed for a smaller nozzle-to-plate spacing. The data with $Z/B = 4$, 10 and 20 are about 46%, 44% and 33% higher than those with $Z/B = 30$, respectively. This trend is consistent with the results of planar air jets [8], as shown in Fig. 5(b). The present data are 20% and 11% higher than those of Gardon and Akfirat [8] for $Z/B = 20$ and 30, respectively, resulting from larger slot width employed in this study and turbulence intensity at the nozzle exit. Gardon and Akfirat [8] found that the turbulence intensity increased from 0.6% to 7.5% with increasing slot width from 1.59 mm to 6.35 mm at $Re = 1.1 \times 10^4$.

The following correlation was recommended for the stagnation heat transfer rate

$$Nu_0 = C_1 Re^{m_1} Pr^{n_1}, \tag{9}$$

where the Prandtl number exponent $n_1 = 2/5$ was adopted for smaller Pr number air jets [20]. The coefficient C_1 and exponent m_1 were obtained by a least-squares technique. Table 2 listed the correlating results, the corresponding standard deviation and the jet Reynolds number. Lower standard deviations indicate that a good agreement exists between the present results and the correlations. For circular jets, Zhou and Ma [21] concluded that the exponent of the correlation Nu–Re characterized the flow pattern of the working liquid there, indicating that a larger turbulence intensity corresponds to higher jet Reynolds number exponent. With the impingement plate held beyond $Z/B = 6$, as seen from Fig. 4(b), the turbulence intensity decreases monotonously with the nozzle-to-plate spacing, leading to a lower jet Reynolds number exponent m there. For example, as the nozzle-to-plate spacing is increased from $Z/B = 10$ to 20, and to 30, the exponent m decreases from 0.644 to 0.635, and to 0.587. However, the coefficient C_1 of the correlation decreases due to decreasing jet momentum, shown in Table 2. Fig. 4(b) also shows that the stagnation turbulence intensity at $Z/B = 10$ has a higher value than that at $Z/B = 4$. Comparison of the jet Reynolds number exponent in Table 2 verified the analysis result of Zhou and Ma [21] again. It should be noted here that the jet Reynolds number exponent of 0.62 at $Z/B = 4$ is almost identical to the values of 0.608 reported for free-surface slot water jets by Zumbrunnen et al. [19] and 0.6 for slot air jets by Sparrow and Wong [10], and close to 0.71 for free-surface slot water jets by Wolf et al. [22].

Table 2
Correlation of the stagnation Nusselt number

Z/B	C_1	m_1	SD	Range of jet Reynolds number
4	0.244	0.620	0.0103	2715–24,723
10	0.184	0.644	0.0099	3100–25,005
20	0.162	0.635	0.0094	3100–25,005
30	0.156	0.587	0.0070	2715–24,723

Variation of the stagnation heat transfer rate with nozzle-to-plate spacing is examined in greater detail in Fig. 6. It is seen from the figure that the variation of Nu_0 with Z/B, which may not be monotonic, exhibits a complex nature depending on jet Reynolds number. At a lower jet Reynolds number of $Re = 3100$, the stagnation heat transfer rate decreases initially with the axial distance from the nozzle exit till $Z/B = 4$ and then increases. Thereafter, it decreases monotonously beyond the peak at $Z/B = 6$. These experimental data were reproduced several times to ensure the repeatability in this work. Similar non-monotonic behavior was also observed with slot air jets by Gardon and Akfirat [8] and Sparrow and Wong [10] at a lower jet Reynolds number. For a higher jet Reynolds number, the peak location remains unchanged even though the magnitude increases significantly. Furthermore, the stagnation heat transfer rate decreases monotonously with decreasing nozzle-to-plate spacing from the peak location. This trend is consistent with the contoured nozzle results of Gardon and Akfirat [8]. Compared with the result of Ref. [8] for $B = 3.175$ mm, the present peak location is located slightly upstream due to the different slot width and the nozzle exit configuration. Gardon and Akfirat [7] and Ma et al. [23] showed that the axial distance of the peak

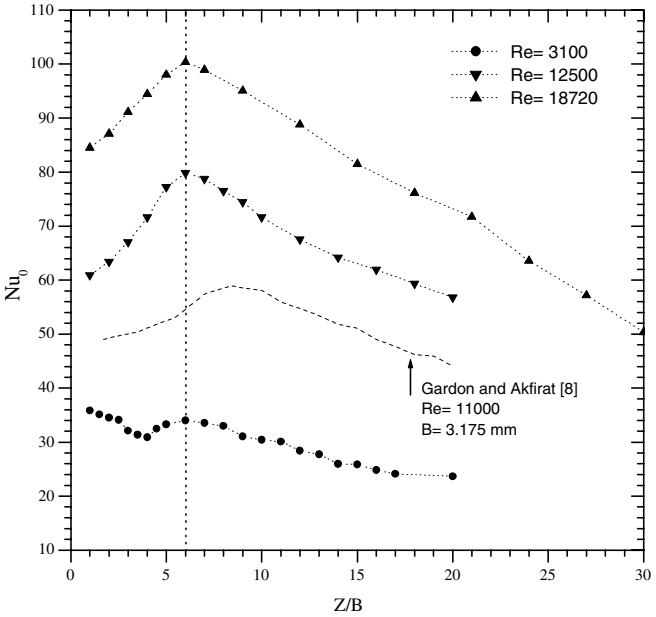

Fig. 6. Variation of the stagnation Nusselt number with the nozzle-to-plate spacing.

decreased with the slot width for air jets and transformer oil jets, respectively.

It is well known that the variation of the stagnation heat transfer with the nozzle-to-plate spacing is mainly affected by two factors: the arrival jet centerline velocity and the turbulence intensity [8,10,24]. At a lower nozzle-to-plate spacing, the heat transfer rate of impinging jet is dominated by the jet velocity because of lower turbulence intensity there. Once leaving the nozzle exit, the jet begins to entrain the surrounding quiescent fluid. Flow visualization measurements showed that the toroidal vortex formed due to an intrinsic instability in the outer shear layer of the impinging jet [3]. As the nozzle-to-plate spacing increases, the potential core width decreases and yet the turbulence intensity increases gradually. For a given jet Reynolds number of $Re = 12{,}500$, as seen from Fig. 4(a), the jet velocity decreases to only $0.8U_e$ at $Z/B = 6$. However, the stagnation heat transfer rate in Fig. 6 reaches its peak there, corresponding to the peak of the turbulence intensity in Fig. 4(b). This shows that convection heat transfer is dominated by the turbulence intensity as the impingement plate is held beyond the potential core. It implies that the variation of stagnation heat transfer rate with nozzle-to-plate spacing is mainly governed by the two conflicting factors.

In order to describe the effect of the free stream turbulence on stagnation Nusselt number, the local values for Re and turbulence intensity Tu measured along the centerline of the free jet (without the impingement plate) were measured and used to correlate the heat transfer data on the impingement plate. The experimental data obtained at the conditions of $5.05\% < Tu < 19.07$ for Z/B values between 1 and 10 are illustrated in Fig. 7, in terms of the parameter $TuRe^{1/2}$. This choice for the combination of the two dimensionless groups was considered to be the most relevant one for the central stagnation line. The local values for Re and Tu on the free jet centerline in the plane of impingement were taken at Z/B equal to that for the plate during the heat transfer tests. The parameter of $Nu/Re^{1/2}$ has a higher value with turbulence intensity, nozzle-to-plate spacing and jet Reynolds number. The local heat transfer rate and the free-stream turbulence intensity of the impingement jet have the following relationship with a standard deviation of 0.0598:

$$\frac{Nu}{Re^{1/2}} = 0.014TuRe^{1/2} + 0.517. \tag{10}$$

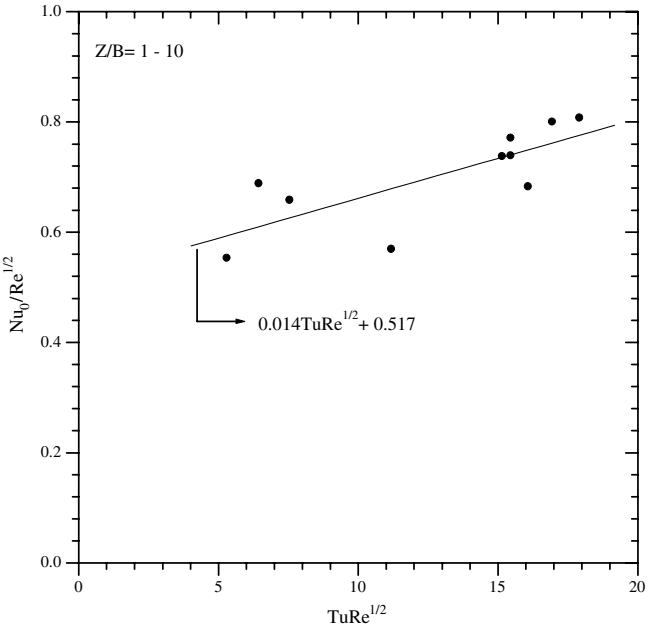

Fig. 7. Correlation of the stagnation heat transfer rate with the turbulence intensity.

Fig. 8(a) and (b) represented the lateral distribution of the local Nusselt number with the same nozzle at $Z/B = 4$ and 10, respectively. The effect of the jet Reynolds number was examined in experimental detail. Fig. 8(a) depicted the variation of the lateral heat transfer rate with respective to the jet Reynolds number in the range of $Re = 2715$–$24{,}723$ at $Z/B = 4$. Except for the case of $Re = 2715$, the general shape of the local Nusselt number distribution is similar, although the magnitude increases with jet Reynolds number. The local heat transfer rate increases initially with lateral distance from the stagnation line and exhibits a peak at around $X/B = 0.35$, which is similar to the result of Ashforth-Frost et al. [11] for slot air jets at $Z/B = 4$. Thereafter, the local heat transfer rate decreases rapidly.

It should be noted here that the lateral distribution of the local Nusselt number has a second peak locating at $X/B = 2.36$–2.89 except for the case of $Re = 2715$. Beyond the peak the local Nusselt number decreases monotonically. As the jet impinges the heater surface, the flow is forced to stagnate and then accelerate radially outward. At a lower nozzle-to-plate spacing, the formation of the convecting wall eddies on the impingement plate produces a larger turbulence intensity, leading a higher heat transfer rate there. The combined effects of the turbulence intensity and the possible transition from laminar to turbulent flow caused the second peak phenomenon. The second peak phenomenon was reported by Sparrow and Wong [10] and Ashforth-Forst et al. [11] for slot air jet and by Ma et al. [23] for slot transformer oil jet, respectively. The second peak occurs only for higher jet Reynolds number and lower nozzle-to-plate spacing, behaving as circular air jet [3,4].

Inspection of Fig. 8(a) shows that the lateral distance of the second peak slightly increases with the jet Reynolds number. The local Nusselt number at the second peak increases with the jet Reynolds number (Fig. 8(a)) and the nozzle-to-plate spacing (Fig. 9). All the local Nusselt number data at the second peak (18 data in all) obtained at $Z/B = 1$–4 were collected and correlated. The correlation with a standard deviation of 0.0203 was given below

$$Nu = 0.138Re^{0.609}(Z/B)^{0.182}. \tag{11}$$

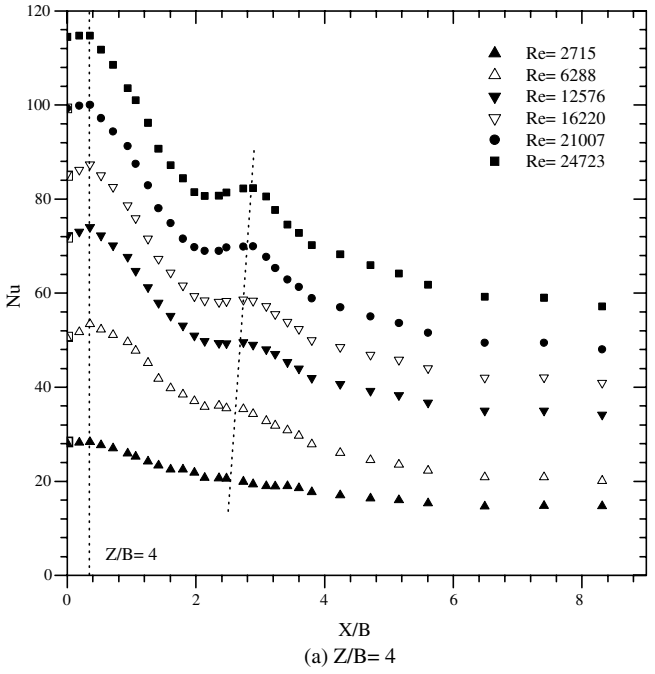

(a) Z/B= 4

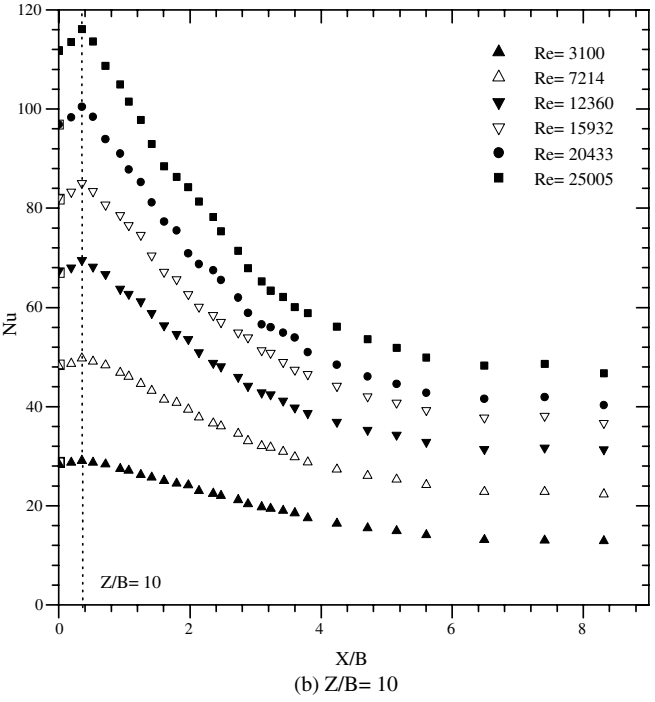

(b) Z/B= 10

Fig. 8. (a, b) Lateral variation of the local Nusselt number at a given nozzle-to-plate spacing: (a) $Z/B = 4$; (b) $Z/B = 10$.

To the best knowledge of the present authors, there is no information on physical explanation of the second peak phenomenon for slot jets in open literature. Further research is required for the occurrence and explanation of the second peak.

Fig. 8(b) illustrated the variation of the lateral heat transfer rate with respective to the jet Reynolds number in the range of $Re = 3100$–$25{,}005$ at $Z/B = 10$. As seen in the figure, the local heat transfer rate increases and reaches a maximum at $X/B = 0.35$, followed a monotonous decreases thereafter. For a given lateral location, the local heat transfer rate increases with the jet Reynolds number. This increase is believed to be more prominent at a smaller lateral distance from the stagnation line. It is worth noting that the lateral location of the first peak remains constant, independent of the nozzle-to-plate spacing and the jet Reynolds number. This location seems to be closely related to the inherent flow structure of impinging submerged air jets. The occurrence of the first peak is mainly attributed to a thin thermal boundary layer, resulting from an accelerated fluid movement outward along the impingement plate.

Fig. 9 illustrated the lateral variation of the local Nusselt number with the nozzle-to-plate spacing at $Re = 12{,}500$. Independent of the nozzle-to-plate spacing, the local heat transfer rate increases initially with the lateral distance from the stagnation line and then decreases beyond the first peak at about $X/B = 0.35$. For a lower nozzle-to-plate spacing of $Z/B \leqslant 4$, the lateral distribution of the local heat transfer rate has two peaks. As the jet goes downstream, the local heat transfer rate at the impingement region increases to a maximum at $Z/B = 6$, and then decreases gradually. It may be well explained by the influence of the jet arrival velocity coupled with the turbulence intensity. It seems that the nozzle-to-plate spacing has a more significant influence on the local Nusselt number at the impingement region. It is also noted that nearly same stagnation region heat transfer rate is obtained at $Z/B = 16$ and 1 despite a larger difference of the axial distance.

In order to illustrate the influence of the jet Reynolds number on the local Nusselt number, average Nusselt number is used in this study to correlate the lateral heat transfer

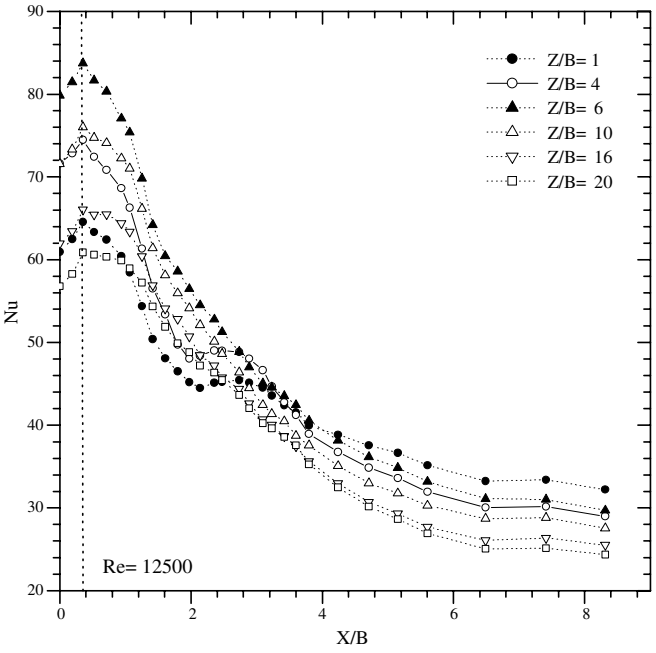

Fig. 9. Lateral variation of the local Nusselt number at $Re = 12{,}500$.

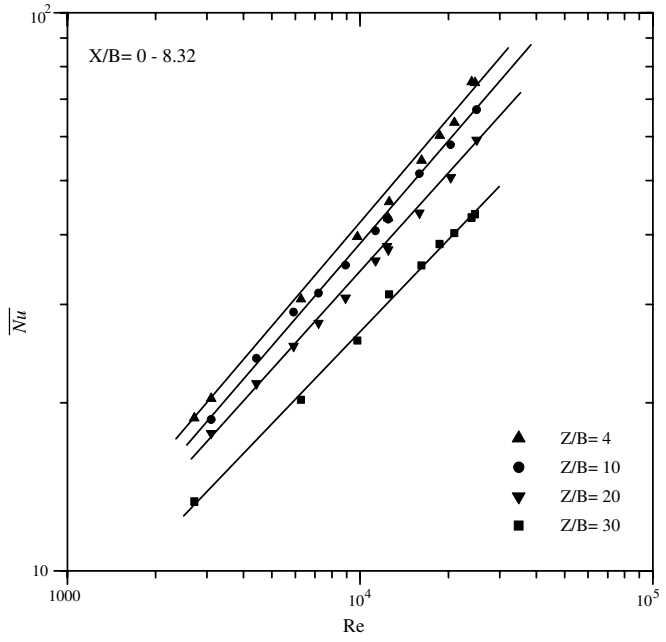

Fig. 10. Variation of the average Nusselt number with respect to the jet Reynolds number for various nozzle-to-plate spacing.

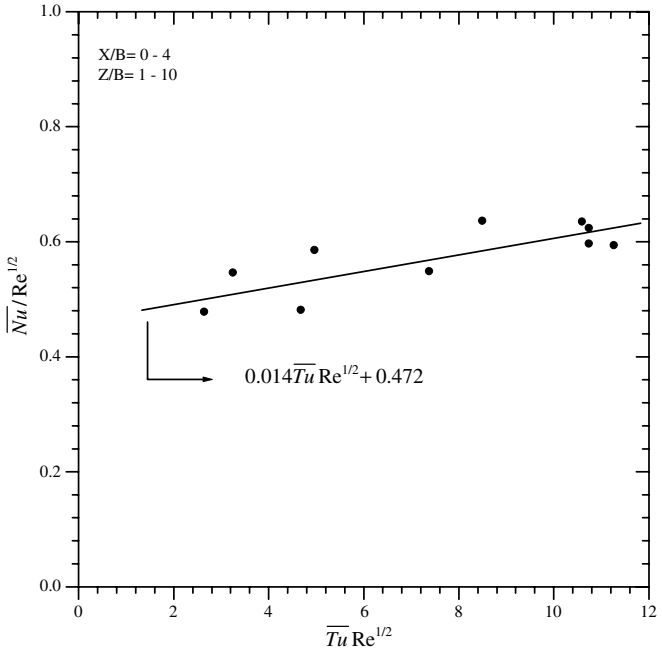

Fig. 11. Effect of the turbulence intensity on average Nusselt number.

rate. The experimental data obtained at $X/B = 0$-8.32 and $Z/B = 4$, 10, 20 and 30 were depicted in Fig. 10. The average Nusselt number increases with the jet Reynolds number and the decrease of nozzle-to-plate spacing. The following correlation was employed to correlate the average heat transfer in the lateral direction

$$\overline{Nu} = C_2 Re^{m_2} Pr^{n_2}, \tag{12}$$

where the Prandtl number exponent $n_2 = 2/5$ was adopted again. The coefficient C_2 and exponent m_2 were obtained by a least-squares technique. Table 3 listed the correlating results. As seen in Table 3, the exponent of the jet Reynolds number decreases with the nozzle-to-plate spacing while the coefficient is in the range of 0.162-0.207. Eq. (12) also reveals a strong dependence of the average Nusselt number on the jet Reynolds number for impinging rectangular air jets.

The correlation between the average Nusselt number and the average turbulence intensity of the impinging jet is illustrated in Fig. 11. The data are for $X/B = 0$-4 and $Z/B = 1$-10. For a given $\overline{Nu}/Re^{1/2}$, the jet with a higher jet Reynolds number has larger values of $\overline{Tu}Re^{1/2}$ than that for lower jet Reynolds number. Independent of the jet Reynolds number and the nozzle-to-plate spacing, the least squares fit yields the following linear relationship between $\overline{Nu}/Re^{1/2}$ and $\overline{Tu}Re^{1/2}$ for values of $2.63 < \overline{Tu}Re^{1/2} < 11.25$ with a standard deviation of 0.0382

$$\frac{\overline{Nu}}{Re^{1/2}} = 0.014\overline{Tu}Re^{1/2} + 0.472. \tag{13}$$

Table 3
Correlation of the average Nusselt number

Z/B	C_2	m_2	SD	Range of jet Reynolds number
4	0.162	0.616	0.0193	2715–24,723
10	0.177	0.599	0.0089	3100–25,005
20	0.207	0.568	0.0085	3100–25,005
30	0.198	0.548	0.0090	2715–24,723

4. Conclusions

Experiments were performed to characterize the fluid flow and heat transfer behaviors produced by impinging air jets exiting a sharp-edged rectangular nozzle. The effects of the jet Reynolds number and the nozzle-to-plate spacing on the local and average Nusselt number of impinging jets were determined to develop an optimum parameter of heat transfer enhancement. The axial and lateral heat transfer data at various test conditions were correlated with a least squares fit, taking into account the effect of the turbulence intensity. The experimental results show that the jet Reynolds number, the nozzle-to-plate spacing and the turbulence intensity have an important influence on the heat transfer of impinging rectangular jets, especially on the impingement region. The present study will provide a better understanding on the fluid flow and heat transfer characteristics of impinging air jets.

Acknowledgements

Support for this work from the Ministry of Science and Technology (MOST) of Korea are gratefully acknowledged.

References

[1] H. Martin, Heat and mass transfer between impinging gas jets and solid surface, Adv. Heat Transfer 13 (1977) 1–60.

[2] R. Viskanta, Heat transfer to impinging isothermal gas and flame jets, Exp. Therm. Fluid Sci. 6 (1) (1993) 111–134.

[3] D.W. Zhou, S.J. Lee, Heat transfer enhancement of impinging jets using mesh screens, Int. J. Heat Mass Transfer 47 (10–11) (2004) 2097–2108.

[4] D.W. Zhou, S.J. Lee, Effect of mesh screen on heat transfer enhancement of impinging jet, J. Enhanced Heat Transfer 12 (1) (2005) 101–119.

[5] Z.H. Lin, Y.J. Chou, Y.H. Hung, Heat transfer behaviors of a confined slot jet impingement, Int. J. Heat Mass Transfer 40 (5) (1997) 1095–1107.

[6] W.H. Schwarz, W.P. Cosart, The two-dimensional turbulent wall jet, J. Fluid Mech. 10 (1961) 481–495.

[7] R. Gardon, J.C. Akfirat, The role of turbulence in determining the heat transfer characteristics of impinging jets, Int. J. Heat Mass Transfer 8 (1965) 1261–1272.

[8] R. Gardon, J.C. Akfirat, Heat transfer characteristics of impinging two dimensional air jets, J. Heat Transfer 88 (1966) 101–108.

[9] D.C. McMurray, P.S. Myers, O.A. Uyehara, Influence of impinging jet variables on local flat surface with constant heat flux, in: J.P. Hartnett (Ed.), Proceedings of the Third International Heat Transfer Conference, 1, Hemisphere Publishing Corporation, 1966, pp. 292–299.

[10] E.M. Sparrow, T.C. Wong, Impingement transfer coefficients due to initially laminar slot jets, Int. J. Heat Mass Transfer 18 (4) (1975) 597–605.

[11] S. Ashforth-Frost, K. Jambunathan, C.F. Whitney, Velocity and turbulence characteristics of a semi-confined orthogonally impinging slot jet, Exp. Therm. Fluid Sci. 14 (1) (1997) 60–67.

[12] V.M. Falkner, S.W. Skan, Some approximate solutions of the boundary layer equation, Philos. Mag. 12 (1931) 865–896.

[13] D.T. Vader, F.P. Incropera, R. Viskanta, Local convective heat transfer from a heated surface to an impinging, planar jet of water, Int. J. Heat Mass Transfer 34 (3) (1991) 611–623.

[14] A.A. Kendoush, Theory of stagnation region heat and mass transfer to fluid jets impinging normally on solid surface, Chem. Eng. Process. 37 (1998) 223–228.

[15] T.H. Park, H.G. Choi, J.Y. Yoo, S.J. Kim, Streamline upwind numerical simulation of two-dimensional confined impinging slot jets, Int. J. Heat Mass Transfer 46 (3) (2003) 251–262.

[16] A.A. Sfeir, The velocity and temperature fields of rectangular jets, Int. J. Heat Mass Transfer 19 (1976) 1289–1297.

[17] W.R. Quinn, Turbulent free jet flows issuing from sharp-edged rectangular slots: the influence of slot aspect ratio, Exp. Therm. Fluid Sci. 5 (1992) 203–215.

[18] S.J. Kline, F.A. McClintock, Describing uncertainties in single-sample experiments, Mech. Eng. 75 (1) (1953) 3–8.

[19] D.A. Zumbrunnen, F.P. Incropera, R. Viskanta, Convective heat transfer distributions on a plate cooled by planar water jets, J. Heat Transfer 111 (3) (1989) 889–896.

[20] C.F. Ma, H. Sun, H. Auracher, T. Gomi, Local convective heat transfer from vertical heated surfaces to impinging circular jets of large Prandtl number fluid, in: G. Hetsroni (Ed.), Proceedings of Ninth International Heat Transfer Conference, vol. 2, Hemisphere Publishing Corporation, Jerusalem, Israel, 1990, pp. 441–446.

[21] D.W. Zhou, C.F. Ma, Radial heat transfer behavior of impinging submerged circular jets, Int. J. Heat Mass Transfer 49 (9–10) (2006) 1719–1722.

[22] D.H. Wolf, R. Viskanta, F.P. Incropera, Local convective heat transfer from a heated surface to a planar jet of water with a nonuniform velocity profile, J. Heat Transfer 112 (1990) 899–905.

[23] C.F. Ma, Y. Zhuang, X.C. Lee, T. Gomi, Impingement heat transfer and recovery effect with submerged jets of large Prandtl number liquid – II: initially laminar confined slot jets, Int. J. Heat Mass Transfer 40 (6) (1997) 1491–1500.

[24] C.S. McDaniel, B.W. Webb, Slot jet impingement heat transfer from circular cylinders, Int. J. Heat Mass Transfer 43 (14) (2000) 1975–1985.